Rate Coefficients and Mechanistic Analysis for Reaction of OH with Vinyl Chloride between 293 and 730 K

Takahiro Yamada, Masud Siraj, and Philip H. Taylor*

Environmental Sciences and Engineering Group, University of Dayton Research Institute, 300 College Park, Dayton, Ohio 43469-0132

Jingping Peng, Xiaohua Hu, and Paul Marshall

Department of Chemistry, University of North Texas, P.O. Box 305070, Denton, Texas 76203-5070

Received: April 24, 2001; In Final Form: July 18, 2001

The kinetics of the title reaction were investigated between 293 and 730 K at 740 ± 10 Torr in a helium bath gas. Absolute rate measurements were obtained using a laser photolysis/laser-induced fluorescence (LP/LIF) technique under slow flow conditions. Rate coefficients exhibited complex behavior with negative temperature dependence at temperatures below 560 K, a rapid drop in rate between 560 and 620 K, and a positive temperature dependence above 620 K. The simple Arrhenius equation adequately describes the data at and below 560 K and is given by (in units of cm^3 $molecule^{-1}$ s^{-1}) $k(293-560\ K) = (2.72 \pm 0.35) \times 10^{-12} \exp(335 \pm 42)/T$. Error limits are 2σ values. The low-temperature values for k are within $\pm 2\sigma$ of the most recent measurements of this reaction obtained under atmospheric pressure conditions. Above 620 K, our measurement combined with the recent measurements of Liu et al.[8] to yield the following rate expression: $k(620-1173\ K) = (6.3 \pm 4.0) \times 10^{-11} \exp(-2740 \pm 490)/T$. Error limits are 2σ values. The rate data were interpreted using variational transition state theory and QRRK theory. OH addition to the β site followed by adduct stabilization describes the low-temperature measurements. Ab initio-based transition state calculations for the H abstraction channel indicated that this mechanism is consistent with the rate measurements above 620 K. H abstraction is predicted to be the dominant reaction channel above temperatures of 800 K.

Introduction

Vinyl chloride (CH_2=CHCl) is used industrially for the production of poly(vinyl chloride) (PVC) and is currently produced at a rate of 27 million tons/year worldwide.[1] Vinyl chloride is classified as a human carcinogen by the EPA[2] and the International Agency for Research on Cancer (IARC).[3] High-temperature incineration remains the best available technology for the complete and permanent disposal of this hazardous material and an important process contributing to the initial destruction of halogenated hydrocarbons is reaction with OH radicals.[4,5]

There are three prior measurements of the reaction of OH with vinyl chloride; two measurements at relatively low temperatures (296 K and 299−423 K, respectively)[6,7] and a more recent measurement between 313 and 1173 K.[8] The mechanism of the reaction of OH radicals with vinyl chloride has been discussed previously by Howard,[6] Perry et al.,[7] Liu et al.,[8] and Atkinson.[9] The mechanism for the initial stages of the reaction can be described by the following reactions

$$OH + CH_2{=}CHCl \leftrightarrow HOC_2H_3Cl^* \qquad (1,-1)$$

$$HOC_2H_3Cl^* + M \leftrightarrow HOC_2H_3Cl + M \qquad (2)$$

The reaction involves the initial addition of OH radicals followed by the stabilization of the OH-vinyl chloride adduct. At sufficiently high pressures, step 2 becomes fast, and the overall loss of [OH] is no longer pressure-dependent. The elimination of a Cl atom is a pathway that can compete with the back reaction (−1)

$$HOC_2H_3Cl^* \rightarrow CH_2{=}CHOH + Cl. \qquad (3)$$

If (3) were fast enough to compete with (−1), the pressure dependence of the addition-initiated reactions would be very small and different behavior would be expected between the reaction of OH with vinyl chloride and the reaction of OH with ethylene. However, prior measurements indicate that the Arrhenius plot of vinyl chloride is very similar to ethylene with a sharp drop in rate constant between ∼575 K and ∼700 K.[8] This behavior implies that in this regime, (−1) becomes fast. This behavior does not, however, necessarily imply that the reaction was at the high-pressure limit at lower temperatures. As a matter of fact, we recently reported QRRK calculations for a similar compound, vinylidene chloride, indicating that OH addition is pressure-dependent at atmospheric pressure at temperatures considerably lower than 600 K.[10] These modeling results are consistent with the data of Howard[6] who reported a pressure dependence for reaction of OH with vinyl chloride at 296 K. As noted by Liu et al.,[8] these studies, performed in 1 to 7 Torr of helium indicated the following: (1) there is a substantial pressure dependence on these rate constants at room temperature suggesting that the rate at room temperature depends significantly on collisional deactivation, (2) the rate constants continue to increase at 7 Torr of helium, thus explaining the lower magnitude of the rate constant compared with Perry et al.[7] and Liu et al.,[8] and (3) the rate constant extrapolated to zero pressure

* To whom correspondence should be addressed. Fax: (937) 229-2503. e-mail: taylorph@udri.udayton.edu.

10.1021/jp011545y CCC: $20.00
Published on Web 09/21/2001

is not large, suggesting that the noncollision-dependent rate is small. These combined experimental and modeling observations suggest that (1,−1) and (2) are dominant at room temperature and moderate pressures and that Cl elimination plays a minor role.

Two possible mechanisms for explaining this behavior were suggested by Perry et al.[7] and Atkinson[9] and subsequently evaluated by Zhu et al.[11] The first is that the OH radical addition only occurs at the β-carbon and the 1,2-migration of OH is rate-determining. The second is that the addition occurs at both the α and β-position, but mainly at the β-position, and the 1,2-migration is sufficiently slow as to be negligible. Because the elimination can proceed directly only when the OH adds at the α-position, the elimination would play only a minor role in the addition-initiated reactions of OH with vinyl chloride. Transition states for the two addition reactions have been characterized by Sekusak et al.,[12] who employed spin-projected MP2 theory with basis sets up to aug-cc-pVTZ and found β addition to be more favorable.

The purpose of this manuscript is to provide further verification of the reaction mechanism of OH radical reactions with vinyl chloride in the form of new atmospheric pressure, extended temperature measurements from 293 to 730 K using the LP-LIF technique. In addition, a refined QRRK analysis of the OH addition reaction mechanism is performed by combining the recent analyses of Zhu et al.[11] with variational transition state theory calculations of the rate of formation of the OH-vinyl chloride adducts. An evaluation of the temperature-dependent rate of H atom abstraction is also performed by utilizing G3 (MP2) ab initio calculations in conjunction with thermochemical transition state theory.[13] The most likely reaction mechanisms based on the modeling of these reaction systems and their consistency with the available experimental data are discussed.

Experimental Approach and Data Reduction

The experimental procedures developed for LP-LIF studies of the reaction of OH radicals with chloroethylenes have been previously published.[14−16] A brief summary is given in the following paragraphs.

To minimize substrate photolysis at wavelengths below 300 nm, HONO was used as a hydroxyl radical source. Parts per million concentrations of pure HONO (>99%) were generated as described by Febo et al.[17] and Brust et al.[18] HONO dissociates primarily into NO and OH when exposed to near-UV radiation of 351 nm. A competing dissociation channel, production of NO_2 and H atoms, has been observed to be negligible under similar experimental conditions.[19] A XeF excimer laser (Lamba Physik Compex model 102) was used as the photodissociation source. Initial $[OH]_0$ ranged over $\sim(3-9) \times 10^{10}$ molecules cm^{-3}, and was determined based on the measured excimer fluence (9−18 mJ cm^{-2}); the most recent published value of the absorption cross-section for HONO, 1.54×10^{-19} cm^2 $molecule^{-1}$ at 351 nm;[18] a quantum yield of unity;[20] and measured values of $[NO_2-]$ taken to represent [HONO] determined using ion chromatography ($\sim(1-3) \times 10^{13}$ molecules cm^{-3}).

Initial substrate concentrations in the reactor, based on measured flow rates, ranged from 1.3×10^{13} to 6.4×10^{14} molecules cm^{-3}. The absence of adsorption on the injector probe (coated with boric acid) and reactor walls was verified using GC/MS analysis. All experiments were conducted at a total pressure of 740 ± 15 Torr with helium as the bath gas. High purity samples (>99%) of vinyl chloride were obtained from Fluka Chemicals. GC/MS analyses indicated the absence of any reactive impurities that would impact the rate measurements.

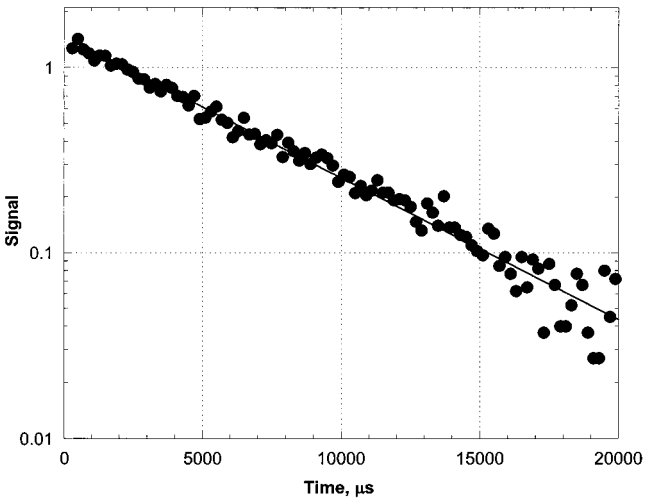

Figure 1. Background-subtracted OH decay profiles at 620 K. $[CH_2{=}CHCl]_0 = 1.48 \times 10^{13}$ molecules cm^{-3}.

The rate of disappearance of the OH may be presented as

$$-d[OH]/dt = k[A_o][OH] + k_d[OH]$$

where k = bimolecular rate constant, A_o = substrate concentration, k_d = first-order rate for the reaction of OH with HONO and also includes diffusion out of the reaction volume.

This relationship holds in the absence of any secondary reactions that may form or deplete OH. Solution of this equation yields $[OH] = [OH]_0 \exp(-k't)$, where $k' = k + k_d$. OH decay measurements were best fit by single exponential decays at all temperatures (relative standard deviations at the 95% confidence interval were = 5% below 620 K and = 10% above 620 K) and were fitted by the following nonlinear expression

$$[OH] = [OH]_0 \exp(-k't) + \gamma$$

where γ is the constant background signal level and t is the time delay between the laser pulses. OH measurements at 560 and 620 K did not exhibit biexponential behavior (see Figure 1 for typical decay profile at 620 K) suggesting that the regime where reformation of OH occurs is a very narrow one for this reaction system. Because the organic concentration was much greater than the [OH], pseudo first-order exponential OH decays were observed and the individual temperature-dependent rate constants were determined by $k' = k[\text{substrate}] + k_d$, where the bimolecular rate constant, k, is the slope of the least-squares fit of k' vs the [organic]. OH decays were measured over two to three decay lifetimes over a time interval of 0.2 to 30.0 ms. Values of k_d measured before and after a rate determination were observed to be constant within experimental uncertainties, indicating that the HONO source was stable over the course of an experiment. Typical values of k_d decreased from $\sim$250 s^{-1} at low temperatures to $\sim$100 s^{-1} at elevated temperatures, suggesting a reduction in the gas-phase concentration of HONO with increasing temperature. Numerical modeling indicated that the dominant source of OH decay in the absence of the substrate was reaction with HONO ($k_{298} = 4.5 \times 10^{-12}$ cm^3 $molecule^{-1}$ s^{-1}).[16] A plot of k' vs substrate concentration at selected temperatures is shown in Figure 2.

Experimental Results

Data were obtained from 293 to 730 K, under atmospheric pressure conditions. OH signals decreased below acceptable

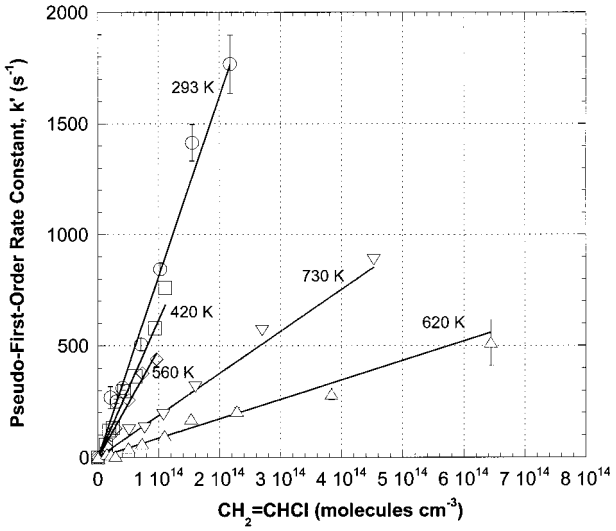

Figure 2. Plot of pseudo-first-order rate constants vs concentration for CH_2═CHCl at five different reaction temperatures. Error bars for the 293 and 620 K data denote $\pm 2\sigma$ random error limits. The baseline decay rate has been subtracted from each measurement.

TABLE 1: Absolute Rate Coefficients for OH + CH_2 = CHCl

T (K)	$k/10^{-12}$ (cm^3·molecule^{-1}·s^{-1})	T (K)	$k/10^{-12}$ (cm^3·molecule^{-1}·s^{-1})
293	8.49 ± 0.40[a]	560	4.84 ± 0.68
360	7.45 ± 0.97	620	0.869 ± 0.132
420	6.16 ± 0.65	650	0.782 ± 0.116
500	5.52 ± 0.66	710	1.09 ± 0.24
550	4.83 ± 0.45	730	1.88 ± 0.19

[a] Errors represent $\pm 2\sigma$ and do not include the 5−10% uncertainty estimated for possible systematic errors.

levels (S/N ratio <10) at higher temperatures, indicating significant thermal decomposition of HONO. Sources of secondary chemistry were not evident based on chemical analysis of the gas stream containing the HONO precursors. Concentrations of NO, NO_2, and HCl were below detection limits (<0.05 ppm). The OH consumption rate was thus controlled by the initial [HONO] which was maintained below 5×10^{13} molecules cm^{-3} to limit the first-order OH decay rate to <300 s^{-1}.

Absolute rate coefficients are presented in Table 1. Random error limits ($\pm 2\sigma$) were below 15% at all temperatures. Rate measurements were collected for a wide range of initial concentrations and included an order of magnitude concentration difference for each series of runs. Substrate partial pressures were measured with a capacitance manometer. Substrate concentrations were based on total flow measurements checked before and after each rate measurement using the soap bubble method.

Previous rate measurements are summarized in Figure 3. Our room-temperature measurements are in agreement with the recent atmospheric pressure measurements of Liu et al.[8] (made with a different bath gas, Ar), given the stated experimental uncertainties, and therefore appear to be at the high-pressure limit. The earlier measurements of Howard[6] and Perry et al.[7] are ~28% and ~22% smaller than our measurements. The trend in rate coefficients is consistent with the influence of pressure on the measured rate and suggests that the measurements of Howard[6] (7 Torr) and Perry et al.[7] (~50 Torr) were obtained under pressure falloff conditions.

Rate coefficient measurements exhibited complex behavior with negative temperature dependence at temperatures below

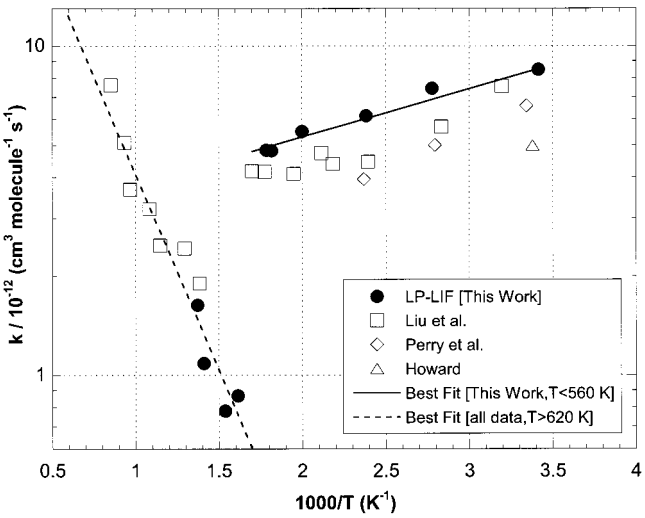

Figure 3. Arrhenius plot of kinetic data for OH + CH_2═CHCl reaction. Also shown are the results of previous studies and an Arrhenius fit to the data from this study (293−560 K) and all available data (620−730 K).

560 K, a rapid drop between 560 and 620 K, and an increase between 620 and 730 K. The simple Arrhenius equation adequately describes the data below 560 K and is given by (in units of cm^3 molecule^{-1} s^{-1})

$$k(293-560\ \mathrm{K}) = (2.72 \pm 0.35) \times 10^{-12} \exp(335 \pm 42)/T$$

Error limits are 2σ values. The negative activation energy derived from an Arrhenius fit to the data below 560 K is slightly lower than prior measurements[7,8] (0.1−0.4 kcal mol^{-1}) and is consistent with the influence of pressure on the reaction. Above 620 K, our measurement, combined with the recent measurements of Liu et al.[8] to yield the following rate expression

$$k\,(620-1173\ \mathrm{K}) = (6.3 \pm 4.0) \times 10^{-11} \exp(-2740 \pm 490)/T$$

Error limits are 2σ values. This expression is in excellent agreement with the Arrhenius expression previously reported by Liu et al.[8]

Theoretical Approach

A detailed theoretical analysis was performed for the following reactions: adduct formation, reverse dissociation, and H atom abstraction.

All ab initio calculations were performed using the Gaussian 98 computer package.[21]

Adduct Formation (C_2H_3Cl + OH → C_2H_3Cl−OH). Variational transition state theory (VTST) calculations were performed to estimate the rate of OH addition to vinyl chloride. The calculations were carried out as follows. First, the reaction coordinates for addition of OH to each end of the C═C bond were defined as intrinsic reaction coordinates (IRCs) at the HF/6-31G(d,p) level. For each IRC, the geometry of the system was optimized at various fixed C−O separations, and frequencies were obtained normal to the IRC, also at the HF/6-31G(d,p) level of theory. Preliminary tests on the OH + C_2H_4 system showed that geometries along the IRC did not depend strongly on the size of the basis set employed, but did vary with the type of correlation treatment. Simple HF results closely ap-

TABLE 2: HF/6-31G(d) Unscaled Frequencies[a]

	$CHClCH_2$	$C\bullet H_2CHClOH$	$C\bullet HClCH_2OH$	$CHClCH_2-OH$ (TS)[b]	$CH_2CHCl-OH$ (TS)[b]	$CH_2CCl-H-OH$ (TS)	$CHClCH-H-OH$ (TS)
1	431	246[c]	106[c]	614i[e]	604i[e]	3298*i*[e]	3234*i*[e]
2	698	317	269	164	123	95	97
3	775	382[d]	372[d]	247	181	142[f]	121[f]
4	1078	437	431	306	299	247	170
5	1093	514	564	429	415	326	327
6	1144	580	885	516	645	511	543
7	1431	696	1048	743	761	641	682
8	1543	995	1166	789	912	717	780
9	1842	1153	1200	946	1003	823	804
10	3352	1273	1287	1051	1041	975	963
11	3426	1405	1375	1119	1142	1102	1029
12	3444	1416	1511	1296	1300	1178	1260
13		1556	1564	1434	1446	1453	1365
14		1617	1652	1608	1626	1535	1527
15		3306	3206	3321	3340	1653	1557
16		3347	3248	3419	3405	3336	3429
17		3464	3402	3434	3440	3434	3431
18		4100	4104	4094	4099	4038	4042

[a] Unit in cm^{-1}. [b] Unscaled HF/6-31G(d,p) frequencies obtained with the 6-31G(d,p) basis set. [c] Corresponding to C—C rotor. [d] Corresponding to C—O rotor. [e] Imaginary frequency. [f] Corresponding to C—HOH rotor.

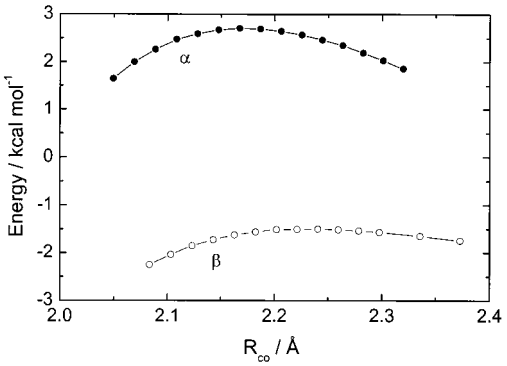

Figure 4. Classical energies (no ZPE) relative to OH + CH_2═CHCl for addition of OH at the CH_2 end (β site, open circles) and the CHCl end (α site, closed circles), calculated at the PMP4/6-311+G(d,p)// HF/6-31G(d,p) level of theory.

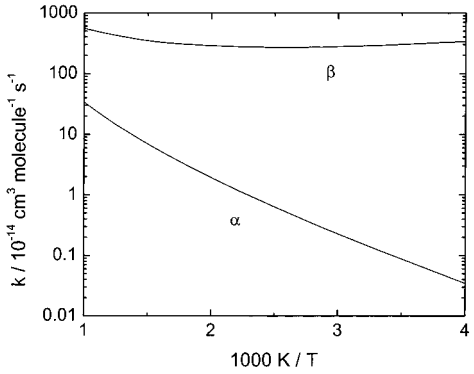

Figure 5. Variational transition state theory rate constants for OH addition to CH_2═CHCl (α and β sites) in units of 10^{-14} cm^3 $molecule^{-1}$ s^{-1}. OH torsion about the forming C—O bond was treated as a vibrator (see text).

proximated the much more demanding QCISD IRC, whereas MP2 data deviated significantly, and therefore HF rather than MP2 data were employed for the VTST analysis of the larger system here. The HF frequencies at the saddle points of the two IRCs are listed in Table 2, and the corresponding geometries are included in Figure 1S. These structures are similar to those obtained by Sekusak et al.,[12] where the greatest differences of 0.06−0.13 Å are associated with the C—O and C—C bonds which change during motion along the IRC. The HF frequencies at points along the IRC were scaled by a factor of 0.90, derived from scaling to match the experimental vibrational frequencies for OH, C_2H_4 and C_2Cl_4.[22] Then energies were computed at the spin-projected PMP4/6-311+G(d,p) level, relative to reactants. These energies, geometries and frequencies were used to derive canonical TST rate constants as a function of position along the IRC. The significant barriers to torsion about the forming C—O bonds in the transition state region, of around 3−4 kcal mol^{-1} at the MP2 level,[12] mean that partition functions for this mode are well-approximated by the vibrational treatment used here. At each temperature, the VTST result was obtained by interpolation to find the minimum rate constant.

These VTST results correspond to the high-pressure limit for OH addition, k_1, equal to the rate coefficient for OH loss when the initially formed excited adduct is always stabilized by collisions. At finite pressures, some fraction of the excited adducts can dissociate back to reactants before collisional stabilization or fragmentation, and thus the observed rate constant is likely to be smaller than the calculated one. At a given pressure, this effect will become more pronounced at elevated temperatures, because the reaction moves further from the high-pressure limit.

The variationally located transition states lie at C—O separations approximately 0.05 Å smaller than the local maxima along the IRCs. As may be seen from Figure 4 for vinyl chloride, the saddle point for β addition lies approximately 1.5 kcal/mol below the reactants' energy, whereas α addition requires overcoming a positive barrier of around +2.7 kcal/mol. The α addition channel is also found to be somewhat less favorable in an entropy context as well (the preexponential factor (AT^ne^n) is approximately 3 times smaller at 298 K). For comparison, we also evaluated Gaussian 3 energies along the RCs which yield barriers about 1 kcal mol^{-1} lower for both channels.[23]

The derived VTST rate constants are plotted in Figure 5. The α channel has a simple positive temperature dependence. The β channel is more important at all temperatures and has a more complex behavior. The negative relative transition state energy implies a negative temperature dependence for the rate constant, an effect which dominates at low temperatures, whereas increases in temperature more rapidly increase the partition function of the loose TS as compared to the reactants, leading to a positive activation energy at higher temperatures.

TABLE 3: G3 Energies of Reactants, Adducts, and Isodesmic Reaction Species at 0 and 298 K[a]

compound	energy at 298 K	energy at 0 K	$\langle S^2\rangle$[b]
C_2H_3Cl	−537.967 729	−537.972 233	
OH	−75.691 601	−75.694 906	0.757
C•H_2CHClOH	−613.709 753	−613.716 040	0.766
C•HClCH_2OH	−613.705 718	−613.711 914	0.766
C_2H_4	−78.503 416	−78.507 418	
C•H_2CH_2OH	−154.238 195	−154.243 702	0.763
CH_2CCl−H−OH (TS)	−613.652 263	−613.659 275	0.878
CHClCH−H−OH (TS)	−613.649 326	−613.656 431	0.884

[a] Unit in Hartree. [b] Obtained with the G3large basis set for open shell compounds.

Reverse Dissociation ($C_2H_3Cl-OH \rightarrow C_2H_3Cl + OH$). The reverse rate constants to form reactants were calculated using the principle of microscopic reversibility (MR). Entropies ($S°_{298}$) and heat capacities ($C_p(T)$, $300 \le T/K \le 1500$) for the reactant (C_2H_3Cl) and vinyl chloride-OH adducts were evaluated using scaled ($\times$ 0.8929) frequencies calculated with HF/6-31G(d) level of theory and geometries optimized by MP2(full)/6-31G(d) level of theory along with statistical mechanics. For all ab initio calculations, singlet species were treated with spin-restricted wave functions, whereas spin-unrestricted wave functions were used for open shell species. The frequencies are shown in Table 2 and the geometries are available as Supporting Information at the end of this manuscript. The calculated vibrational frequencies corresponding to the internal rotational mode (C−C and C−O rotors) were omitted from the $S°_{298}$ and $C_p(T)$ calculations. Instead, the internal rotational treatment advanced by Pitzer and Gwinn was used.[24] The rotational barrier heights for each rotor were calculated from a relaxed scan of the dihedral angle in 15° steps with UHF/6-31G(d) level of theory starting from the optimized configuration, which has lowest energy. The geometries were fully optimized except the scanning dihedral angle. The derived barrier heights were used to calculate the hindered internal rotational contribution for $S°_{298}$ and $C_p(T)$. The well-depth of the addition reactions (α- and β-) was estimated based on C−OH bond dissociation energies (BDEs) of vinyl chloride-OH adducts. The BDEs of vinyl chloride-OH adducts were calculated using the following isodesmic reaction and the experimentally derived C−OH BDE of C•H_2CH_2OH[25]

$$C_2H_3Cl + C_2H_4-OH \text{ adduct} \rightarrow C_2H_4 + C_2H_3Cl-OH \text{ adduct} \quad (4)$$

We viewed the heats of reaction at 0 K ($\Delta H°_{rxn,0}$) in reaction 4 as a difference in the two C−OH BDEs, with the BDE of C_2H_4−OH at 0 K being known.[25] The composite ab initio calculation theory, G3,[23] was used to calculate $\Delta H°_{rxn,0}$. This procedure gives the BDE of C_2H_3Cl−OH directly without needing any additional experimental information. The calculated G3 energy is listed in Table 3. Thermodynamic properties of the OH radical ($\Delta H_f°_{298}$, $S°_{298}$, and $C_p(T)$, $300 \le T/K \le 1500$) and $\Delta H_f°_{298}$ of vinyl chloride were obtained from the literature.[22,26]

The rate of reverse dissociation at the each temperature ($300 \le T/K \le 2000$) was estimated using the forward rate constant derived by VTST and the equilibrium constants calculated based on the thermodynamic properties described above. The rate constants were fit by the following expression:

$$k_{-1} = BT^n \exp(-C/RT)$$

H Abstraction ($C_2H_3Cl + OH \rightarrow C_2H_2Cl + H_2O$). Hydrogen abstraction reactions were calculated using Transition State Theory (TST).[13,27−29] The rate expression for the H abstraction reaction as summarized by Zhu et al.[11] is given by

$$k(T) = 1.3 \times 10^{13}\, T^2 \exp(\Delta S^{\ddagger}/R) \exp(-E_a/RT) \times (\text{reaction degeneracy}), \quad (5)$$

where the reaction degeneracy was set to 2 for the CH_2 carbon site and 1 for the CHCl site. $S°_{298}$ and $C_p(T)$ ($300 \le T/K \le 1500$) for the H abstraction TS were calculated in the same manner as those for the C_2H_3Cl−OH adducts. The CC−HOH rotor was treated as a hindered internal rotor. The rotational barrier heights were calculated by scanning the dihedral angle at 15° intervals with UHF/6-31G(d) level of theory starting from the optimized configuration. A fixed geometry was used during the scan. The frequencies are shown in Table 2 and the geometries are available as Supporting Information at the end of this manuscript. The activation energies were derived from the energy difference between the reactants and TSs calculated by G3,[23] which are shown in Table 3.

Reaction Mechanism and Quantum Rice Ramsperger Kassel (QRRK) Analysis. The calculated adduct formation, reverse dissociation, and H abstraction rate constants were combined with the reaction mechanism developed by Zhu et al.[11] Quantum Rice Ramsperger Kassel (QRRK) analyses[30,31] for $k(E)$ combined with the master equation for falloff[32] were used to predict chemically activated pressure-dependent rate constants. $\langle DE\rangle_{down}$ of 210 cm^{-1} (600 cal mol^{-1}) was used for master equation analysis. This value is within the range of values recently derived by Knyazev and Tsang[33] in their weak collision master equation modeling of experimental measurements of the decomposition of *sec*-butyl radicals between 170 and 373 K.

Modeling Results

Table 2 shows calculated frequencies at the HF/6-31G(d) level of theory without scaling. The frequencies omitted from the $S°_{298}$ and $C_p(T)$ calculations are also indicated. According to a vibrational mode analysis, the lowest and third lowest frequencies corresponded to the C−C and C−O rotors, respectively, for the vinyl chloride-OH adducts, whereas the second lowest frequencies corresponded to C−HOH rotors for H abstraction TSs. The calculated C−H and H−O bond lengths and C−H−O bond angle were 1.243 Å, 1.215 Å, and 160.0°, respectively, for the CH_2CCl−H−OH TS geometry. Those for the CHClCH−H−OH TS were 1.257 Å, 1.197 Å, and 157.7°, respectively. Because of the wide ∠C−H−O bond angle, C−H and H−OH rotors were represented as one C−HOH rotor to calculate the rotational barrier height and to estimate the hindered internal rotational contribution for $S°_{298}$ and $C_p(T)$. Two minima were observed for the C−C and C−O rotors in the C•H_2CHClOH adduct, whereas three minima were observed for the C−C and C−O rotors in the C•HClCH_2OH adduct. A single minima was observed for C−HOH rotor in the H abstraction TSs. The rotational barriers were averaged for the C−C and C−O rotors. The calculated rotational barriers of C−C and C−O for C•H_2CHClOH were 1.15 and 3.52 kcal mol^{-1}, respectively, whereas those for C•HClCH_2OH were 2.23 and 2.24 kcal mol^{-1}, respectively. The rotational barrier of the C−O rotor for C•H_2CH_2OH was also calculated with the same ab initio method and it shows 3 maxima with an average height of 2.07 kcal mol^{-1}. The rotational barrier of the C−O rotor for C•H_2CHClOH was higher compared with the other two. It is conceivable that the relatively high rotational barrier is due, in part, to a H−Cl interaction (2.759 Å). The H−Cl interaction is consistent with a lower energy for the α-adduct compared with the β-adduct.

TABLE 4: Thermodynamic Properties

compound		$\Delta H_f^\circ{}_{298}$[d]	$S^\circ{}_{298}$[e]	C_{p300}[f]	C_{p400}	C_{p500}	C_{p600}	C_{p800}	C_{p1000}	C_{p1500}	symmetry no.
C_2H_3Cl		5.5	63.03	12.83	15.47	17.69	19.52	22.3	24.33	27.46	1
OH		9.4	43.88	7.17	7.09	7.06	7.06	7.15	7.33	7.87	1
C•H_2CHClOH											2
	TVR[a]		67.49	16.40	19.63	22.31	24.48	27.78	30.2	34.05	
	IR[b]		7.89	3.59	3.52	3.37	3.18	2.85	2.62	2.32	
	total[c]	−20.9	76.76	19.99	23.15	25.68	27.66	30.63	32.82	36.37	
C•HClCH_2OH											1
	TVR		68.00	15.04	18.32	21.20	23.59	27.23	29.86	33.93	
	IR		10.24	4.02	3.76	3.42	3.14	2.75	2.52	2.24	
	total	−17.6	79.62	19.06	22.08	24.62	26.73	29.98	32.38	36.17	
CH_2CCl−H−OH (TS)			79.62	19.06	22.08	24.62	26.73	29.98	32.38	36.17	1
	TVR		74.73	19.24	22.51	25.08	27.09	29.99	32.04	35.18	
	IR		4.07	1.74	1.50	1.35	1.25	1.15	1.10	1.04	
	total	19.3	80.18	20.98	24.01	26.43	28.34	31.14	33.14	36.22	
CHClCH−H−OH (TS)											1
	TVR		74.47	19.21	22.55	25.16	27.18	30.06	32.08	35.19	
	IR		4.25	1.49	1.31	1.21	1.15	1.08	1.05	1.02	
	total	21.2	80.10	20.70	23.86	26.37	28.33	31.14	33.13	36.21	

[a] Translational, rotational, and vibrational contribution for S°_{298} and $C_p(T)$, symmetry number was taken into account for S°_{298} calculation (1.987 × ln(number of symmetry) cal/(mol K)). [b] Hindered internal rotational contribution for S°_{298} and $C_p(T)$. [c] Electronic degeneracy was taken into account for S°_{298} calculation. [d] Unit in kcal/mol. [e,f] Unit in cal/(mol K).

TABLE 5: Calculated Rate Expression

	$k = B\,T^n \exp(-C/RT)$			
reaction	B[a]	n	C[b]	note
$C_2H_3Cl + OH \rightarrow C•H_2CHClOH$	1.00×10^{-19}	2.35	2.4	VTST
$C•H_2CHClOH \rightarrow C_2H_3Cl + OH$	3.67×10^{10}	0.91	30.6	MR
$C_2H_3Cl + OH \rightarrow C•HClCH_2OH$	1.25×10^{-18}	2.10	−2.2 (−1.6)[c]	VTST
$C•HClCH_2OH \rightarrow C_2H_3Cl + OH$	3.67×10^{10}	0.91	30.6	MR
$C_2H_3Cl + OH \rightarrow CH_2C•Cl + H_2O$	1.82×10^{7}	2.00	4.4	TST
$C_2H_3Cl + OH \rightarrow CHClC•H + H_2O$	3.50×10^{7}	2.00	6.3	TST

[a] Unit in s^{-1} for unimolecular reaction or cm^3 molecule^{-1} s^{-1} for bimolecular reaction. [b] Unit in kcal mol^{-1}. [c] Number calculated (in parentheses) is adjusted to fit experimental data.

The calculated rotational barriers for the H abstraction TS were 1.29 and 0.97 kcal mol^{-1} for CH_2CCl−H−OH and CHClCH−H−OH, respectively.

Table 3 shows calculated G3 energies at 0 and 298 K for reactants, vinyl chloride-OH adducts, H abstraction TSs, and several compounds used in isodesmic reactions to calculate the BDEs of vinyl chloride-OH adducts. On the basis of the isodesmic reactions, $\Delta H^\circ_{rxn,0}$ for C•H_2CHClOH and C•HClCH_2OH were calculated as −5.4 and −2.1 kcal mol^{-1}, respectively. On the basis of the BDE at 0 K for $C_2H_4 + OH \rightarrow C•H_2CH_2OH$[21] of 29.4 ± 1.4 kcal mol^{-1}, the BDE (0 K) for C•H_2CHCl−OH and C•HClCH_2−OH were calculated as 34.8 and 31.5 kcal mol^{-1}, respectively. The thermal corrections for OH, C_2H_3Cl, C•H_2CHClOH, and C•HClCH_2OH, calculated with (U)HF/6-31G(d) determined frequencies, were 2.1, 2.8, 3.9, and 3.9 kcal mol^{-1}, respectively. (This implies that the BDE at 298 K is 1.0 kcal mol^{-1} larger than the BDE at 0 K.) This leads to a BDE at 298 K for C•H_2CHCl−OH and C•HClCH_2−OH of 35.8 and 32.5 kcal mol^{-1}, respectively. These values are consistent with the values of Zhu et al.[11] (36.1 and 32.7 kcal mol^{-1} for C•H_2CHClOH and C•HClCH_2OH, respectively), based on the B3LYP/6-31G(d,p) level of theory and a different isodesmic reaction. The activation energies for H abstraction reactions (CH_2CCl−H−OH and CHClCH−H−OH) were estimated as 4.43 and 6.28 kcal mol^{-1}, respectively.

The calculated thermodynamic properties are shown in Table 4. TVR indicates translational, vibrational, and rotational contribution for S°_{298} and $C_p(T)$ ($300 \le T/K \le 1500$) and IR indicates hindered internal rotational contribution for S°_{298} and $C_p(T)$ ($300 \le T/K \le 1500$). The symmetry number was taken into account in the S°_{298} of TVR, and the electronic degeneracy was taken into account in the S°_{298} of the total value. $\Delta H_f^\circ{}_{298}$ for the vinyl chloride-OH adducts were estimated based on C−O BDE calculations described earlier. $\Delta H_f^\circ{}_{298}$ for the H abstraction TSs were calculated based on $\Delta H_f^\circ{}_{298}$ of reactants and G3 energy difference between reactants and TSs.

The calculated high-pressure limit rate constants for OH addition to vinyl chloride, reverse dissociation, and H abstraction reaction are listed in Table 5. The variationally located TS energy for β addition, at the PMP4/6-311+G(d,p) level, was decreased by 0.6 kcal mol^{-1} to fit the experimental results. Figure 6 presents a comparison of the experimental data with the QRRK predicted forward rate coefficient in Arrhenius form at $p_{He} = 1$ atm. The agreement between the total forward rate for the β channel and the available atmospheric pressure measurements between 293 and 560 K is excellent. Figure 6 also shows the QRRK estimated temperature-dependent reaction rate constants for specific pathways. For this temperature range the predicted dominant product is $CHClCH_2OH$, formed by OH addition to the β site followed by collisional stabilization. The reverse reaction (not shown) is dominant above 600 K and is consistent with the rapid drop-off in the observed bimolecular rate coefficients between 560 and ~620 K. Chemically activated OH addition pathways were insignificant below 1000 K. Above 1000 K, OH addition to the α site followed by Cl elimination is a minor channel yielding vinyl alcohol as a stable product. Another minor channel above 1500 K is OH displacement of H yielding chlorovinyl alcohol as a stable product. These

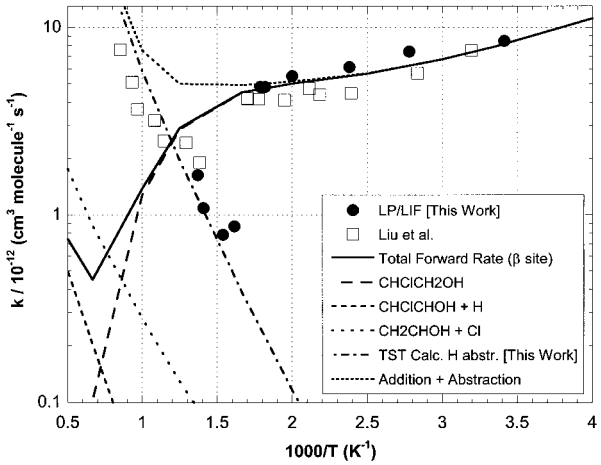

Figure 6. Arrhenius plot of the QRRK model results ($p_{He} = 1$ atm). Shown are the LP-LIF experimental measurements from this work, the experimental measurements of Liu et al.,[8] the total forward rate (β site), $CHClCH_2OH$ formation rate, H elimination rate, Cl elimination rate, ab initio-based TST calculation of the H atom abstraction channel (sum of α- and β-H abstraction channels), and the sum of the OH addition and H abstraction channels.

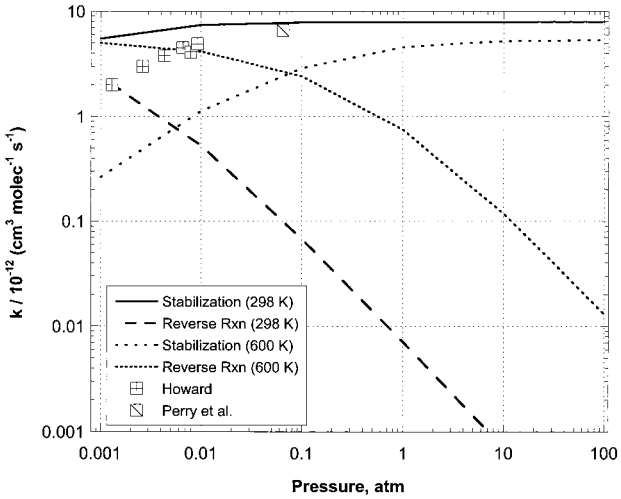

Figure 7. Arrhenius plot of the QRRK model results at 0.001, 0.01, and 0.1 and 1 atm. Shown are the adduct stabilization channel (β site) and the reverse reaction at 298 and 600 K and the previous measurements of Howard[6] and Perry et al.[7] at sub-atmospheric pressures.

reactions are insignificant at high temperatures compared to the dominant H atom abstraction channel (see below).

We can use the observed drop in rate coefficient around 600 K to make a crude estimate of the thermochemistry of the β-adduct. For a general scheme

$$A + B \leftrightarrow C$$

with initial conditions [A] ≪ [B] and [C] = 0, then with f as the fraction of A consumed, at equilibrium the concentration equilibrium constant K_c is equal to $[B]^{-1}f/(1 - f)$. At 560 K, we assume at least half the OH was consumed by adduct formation ($f > 0.5$) at the lowest vinyl chloride concentrations employed (see Figure 2) which implies $K_c > 6.7 \times 10^{-14}$ molecule^{-1} cm^3. Together with $\Delta S = -27.3$ cal mol^{-1} K^{-1} derived from Table 4, this yields $\Delta H < -30.5$ kcal mol^{-1}. Similarly, assuming less than half the OH is consumed by adduct formation at 620 K leads to $K_c < 1.6 \times 10^{-15}$ molecule^{-1} cm^3. Together with $\Delta S = -27.3$ cal mol^{-1} K^{-1} this implies $\Delta H > -33.6$ kcal mol^{-1}. We note that this simple analysis brackets the C−O BDE in the adduct, but shows that values around 30.5 to 33.6 kcal mol^{-1} are consistent with the kinetics. ΔC_p is small (Table 4) and the corresponding BDE at 298 K would be about 32 kcal mol^{-1}. This rough estimate is in reasonable agreement with our computed value of 32.5 kcal mol^{-1}, and also compares favorably with the values of 32.7 and 33.4 kcal mol^{-1} derived by Zhu et al.[11] and Sekusak et al.[12]

Figure 6 also presents transition state theory (TST) calculations for the respective H atom abstraction channel for vinyl chloride. Our calculated activation energies using G3[23] theory are 0.63 and 1.89 kcal mol^{-1} higher than the values proposed by Zhu et al., which were estimated using Evans−Polanyi plot for several chlorinated hydrocarbons.[11] Our calculated entropy difference between the reactants and the TSs were 1.3 and 1.5 cal mol^{-1} K^{-1} lower than the values proposed by Zhu et al.[11] They analyzed the change of bond lengths and angles, vibrational frequencies, internal rotor parameter, electronic degeneracy, and symmetry properties using thermochemical TST.[13,27−29] Regardless of the different calculational approach, our results showed good agreement with our experimental measurements between 620 and 730 K and the higher temperature measurements of Liu et al.[8]

Figure 7 illustrates the effect of pressure on the QRRK estimated adduct stabilization reaction (and the reverse reaction). Also included are the measurements of Howard[6] and Perry et al.[7] performed at room temperature. The modeling results indicate that their measurements[6,7] were obtained in the falloff region at temperatures at and above room temperature. The agreement between QRRK predictions and prior experiments is good above 0.01 atm with a larger deviation evident at lower pressures.

Comparison with Previous Modeling Results

The only previous modeling study, that of Zhu et al.,[11] reported that OH addition to the α-carbon was a low fraction, ca. 10%, of that for addition to the β carbon at room temperature under 1 atm. Our estimates, based on VTST calculation of the respective barrier height, indicate that OH addition to the α-carbon at room temperature is negligible, i.e., less than 0.01% of the measured rate.

Formation of the β-stabilized adduct is the dominant addition product at 1 atm from 298 to 1000 K, as reported by Zhu et al. Our calculations show that the β-stabilization rate constant decreases with increasing temperature because at fixed pressure, the system moves deeper into the pressure falloff region as the temperature is raised. By contrast, the overall forward rate coefficient for OH addition to the α site increases with temperature. The calculations of Zhu et al. imply that OH addition to the α site goes entirely to the vinyl alcohol + Cl channel at a constant rate over the entire temperature range (298−2000 K). In other words, this reaction occurs essentially without any barrier. Our calculations indicate that adduct stabilization occurs to a significant degree at room temperature and lower temperatures with the Cl elimination channel dominating above 400 K. The essential difference between the two calculations is that our VTST calculations indicate a small barrier to OH addition at the α-site. There are several recent estimates of the A factor for the elimination of Cl atoms from hydrocarbon adducts. Zhu et al.[11] used a value of 2.8×10^{12} s^{-1} in their model for C•H_2CHClOH based on a MOPAC/PM3 calculation. Alternatively, Barat and Bozzelli[34] proposed a value of 3.9×10^{13} s^{-1} based on a TST calculation for Cl elimination from β-chloroethyl radical. Knyazev et al.[35] derived a a high-pressure limit value of 1.7×10^{14} s^{-1} based on a master equation

collisional analysis of Cl elimination from β-chloroethyl radical. This latter value is within a factor of 3 of our simple collision theory estimate of the rate of Cl elimination from $C\bullet H_2CHClOH$ (6.0×10^{14} s^{-1} at 600 K). At room temperature, and with this collision theory-based A factor for Cl elimination, our computed barrier to α addition makes the branching ratio for Cl production equal to 0.00014. This is considerably smaller than reported experimental values of 4-9%.[6−8,36,37] Even reducing the alpha addition barrier to zero, i.e., by 2.7 kcal mol^{-1}, yields a branching ratio of only 0.008. The experimental data may therefore be somewhat overestimated. The reverse reaction of the β-adduct, dissociation to vinyl chloride + OH, increases with temperature and dominates stabilization above ca. 600 K. This result is consistent with our measurements and with the prior calculations of Zhu et al.

The α-adduct channel behaves differently from β-addition due to the positive energy barrier for OH addition and the presence of low-energy reaction channels available to this adduct, specifically, Cl elimination. There are two pathways that result in vinyl alcohol formation, one direct path, and a second indirect path that requires a Cl shift. We calculate that the vinyl alcohol + Cl products dominate the α-addition channel from 400 to 2000 K.

Our TST calculations and the calculations of Zhu et al. indicate that H atom abstraction dominates the experimental measurements at elevated temperatures. Our calculations indicate that the abstraction reaction begins to dominate over addition above 800 K, in good agreement with the observations of Zhu et al. The QRRK calculations of the OH addition rate constants and the TST calculations for the H atom abstraction rate constants (α and β sites) yield cumulative rate coefficients that are in good agreement with experimental data spanning a range of 293−1173 K (see Figure 5).

Comparison with Other Chloroethylenes

This study concludes our analysis of the reaction of hydroxyl radicals with the chloroethylenes.[10,14−16] The temperature dependence of the measurements varied significantly with chlorine substitution. We observed that the energy of the initial OH addition transition states (relative to reactants) plays a significant role in determining the temperature dependence of these reactions. For tetrachloroethylene, the energy of the initially formed OH addition transition state lies ca. 1 kcal mol^{-1} *above* the energy of the reactants, thus explaining the reduced reaction rate and the positive temperature dependence of the reaction. This is in contrast to OH addition to trichloroethylene and 1,2-dichloroethylene, where the energy of the transition state for the dominant reaction channel (β site) is below the energy of the reactants. The order of magnitude increase in room-temperature rate constant for trichloroethylene and 1,2-dichloroethylene vs tetrachloroethylene is due, in part, to the relative energies of the initial transition states. Furthermore, the factor of 4 to 5 increased room-temperature reactivity for vinyl chloride and vinylidene chloride vs 1,2-dichloroethylene is once again due, in part, to the lower energy of the transition states (β site) relative to reactants.

Vinyl chloride and vinylidene chloride exhibited the often-observed negative-temperature dependent behavior of OH addition reactions at low temperatures with a reaction mechanism dominated by OH addition. The observed temperature dependence reflects the importance of collisional processes in the stabilization of the OH addition adduct. *trans*-1,2-Dichloroethylene, trichloroethylene, and tetrachloroethylene exhibited atypical temperature-dependent behavior that is indicative of a more complex reaction mechanism involving competition between adduct stabilization and chlorine elimination. Chlorine elimination was observed to dominate the tetrachloroethylene reaction with adduct stabilization playing minor roles at low temperatures for trichoroethylene and 1,2-dichloroethylene. At elevated temperatures, evidence for H atom abstraction mechanisms was observed for vinyl chloride and vinylidene chloride. This dramatic change in temperature dependence of the rate constants was not clearly resolved for *trans*-1,2-dichloroethylene and trichloroethylene due to the dominance of a more rapid chlorine elimination reaction.

The results of these studies indicate that OH addition/Cl elimination is a significant pathway for the oxidation of 1,2-di-, tri-, and tetrachloroethylene under postcombustion conditions. Detailed modeling of these reaction systems indicated that chlorinated vinyl alcohols and chlorinated acid chlorides are expected to be the primary reaction products from the OH radical initiated oxidation of these compounds. Evidence for these pathways through the formation of 1,1-dichloroethenol has been recently demonstrated in laboratory studies of trichloroethylene combustion.[38] At temperatures above 1000 K, H atom abstraction will be the dominant oxidation pathway for all hydrogen-containing chloroethylenes. The resulting products will decompose through β-Cl scission yielding acetylene and chloroacetylene products. In contrast to the chlorovinyl alcohols, these products are of environmental concern due to their special reactivity under the appropriate low-temperature, postcombustion conditions. Recent studies by one of the authors have shown that these thermally stable compounds under gas-phase conditions are precursors for chloroaromatic and PCDD/F formation at low temperatures (423−673 K) through interaction with surfaces that contain small amounts of copper species.[39−41]

Summary

New, atmospheric pressure, rate coefficient measurements are presented for the reaction of OH radicals with vinyl chloride. The new rate measurements (and modeling results) are consistent with prior lower and higher temperature measurements. The data below 600 K were successfully modeled by conducting an ab initio-based reaction pathway analysis based on an OH addition mechanism. Variational TST calculations of the entrance channel were consistent with the experimental measurements. β-Adduct stabilization was found to be the dominant mechanism below 560 K, hence the observed negative temperature dependence. Ab initio-based TST calculations for the respective H-abstraction channels indicated that this mechanism is important at temperatures above 800 K. At flame temperatures, H atom abstraction will be the dominant mechanism of OH attack. H- and Cl-atom elimination pathways are of minor importance at combustion temperatures.

Acknowledgment. The authors acknowledge support from the Environmental Protection Agency (Grant R82-6169-01-0). Although this research has been supported by the US-EPA, it has not been subject to Agency review and therefore does not necessarily reflect the views of the Agency, and no official endorsement should be inferred. P.M. also thanks the R.A. Welch Foundation (Grant B-1174) and UNT for support. Some of the calculations were performed on the National Center for Supercomputing Applications SGI/Cray Origin 2000 (Grant CHE000015 N).

Supporting Information Available: Figure 1S (a)−(d) presents MP2(full)/6-31G(d) optimized geometries for the OH

addition adducts and the H atom abstraction transition states. Figure 1S (e)−(f) present HF/6-31G(d,p) optimized geometries for the OH addition transition states. This material is available free of charge via the Internet at http://pubs.acs.org.

References and Notes

(1) Kielhorn, J.; Melber, C.; Wahnschaffe, A.; Mangelsdorf, I. *Environ. Health Perspect*. **2000**, *108*, 579.

(2) U. S. Environmental Protection Agency, 1990. Clean Air Act of **1990**, 42USC.7412, Title I, Part A, Sec. 112, 53.

(3) International Agency for Research on Cancer, 1979. Monographs on the Evaluation of the Carcinogenic Risk of Chemicals to Humans, Vol. 19, IARC, World Health Organization, Lyon France.

(4) Fairchild, P. W.; Smith, G. P.; Crosley, D. R.; *Proc. Combust. Inst., Vol. 19*, The Combustion Institute, p 107, 1982.

(5) Warnatz, J.; Bockhorn, H.; Moser, A.; Wenz, H. W. *Proc. Combust. Inst., Vol. 19*, The Combustion Institute, p 197, 1982.

(6) Howard, C. J. *J. Chem. Phys.* **1976**, *65*, 4771.

(7) Perry, R. A.; Atkinson, R.; Pitts, J. N., Jr. *J. Chem. Phys.* **1977**, *67*, 458.

(8) Liu, A.; Mulac, W. A.; Jonah, C. D. *J. Phys. Chem.* **1989**, *93*, 4092.

(9) Atkinson, R. *J. Phys. Chem. Ref. Data*, **1989**, Monograph 1.

(10) Yamada, T.; El-Sinawi, A.; Siraj, M.; Taylor, P. H.; Peng, J.; Hu, X.; Marshall, P. *J. Phys. Chem. A.* **2001**, accepted for publication.

(11) Zhu, L.; Bozzelli, J. W.; Ho, W.-P. *J. Phys. Chem. A* **1999**, *103*, 7800.

(12) Sekušak, S.; Liedl, K. R.; Sabljić, A.; A. *J. Phys. Chem. A* **1998**, *102*, 1583.

(13) Cohen, N.; Benson, S. W. *J. Phys. Chem.* **1987**, *91*, 162.

(14) Tichenor, L. B.; Taylor, P. H.; Yamada, T.; Peng, J.; Hu, X.; Marshall, P. *J. Phys. Chem. A.* **2000**, *104*, 1700.

(15) Tichenor, L. B.; El-Sinawi, A.; Taylor, P. H.; Yamada, T.; Peng, J.; Hu, X.; Marshall, P. *Chemosphere* **2001**, *42*, 571.

(16) Tichenor, L. B.; Lozada-Ruiz, A. J.; Yamada, T.; El-Sinawi, A.; Taylor, P. H.; Peng, J.; Hu, X.; Marshall, P. *Proc. Combust. Inst.* **2001**, *28*, 1495.

(17) Febo, A.; Perrino, C.; Gherardi, M.; Sparapani, R. *Environ. Sci. Technol.* **1995**, *29*, 2390.

(18) Brust, A. S.; Becker, K. H.; Kleffmann, J.; Wiesen, P. *Atmos. Environ.* **2000**, *34*, 13.

(19) Wollenhaupt, M.; Carl, S. A.; Horowitz, A.; Crowley, J. N. *J. Phys. Chem.* **2000**, *104*, 2695.

(20) Cox, R. A. *J. Photochem.* **1974**, *3*, 175.

(21) Frisch, M. J.; Trucks, G. W.; Schlegel, H. B.; Scuseria, G. E.; Robb, M. A.; Cheeseman, J. R.; Zakrzewski, V. G.; Montgomery, J. A.; Stratmann, R. E.; Burant, J. C.; Dapprich, J. M.; Millan, J. M.; Daniels, A. D.; Kudin, K. N.; Strain, M. C.; Farcas, O.; Tomasi, J.; Barone, V.; Cossi, M.; Cammi, R.; Mennucci, B.; Pomelli, C.; Adamo, C.; Clifford, S.; Ochterski, J.; Petersson, G. A.; Ayala, P. Y.; Cui, Q.; Morokuma, K.; Marick, D. K.; Rabuck, A. D.; Raghavachari, K.; Foresman, J. B.; Cioslowski, J.; Ortiz, J. V.; Stefanov, B. B.; Liu, G.; Liashenko, A.; Piskorz, P.; Komaromi, I.; Gomperts, R.; Martin, R. L.; Fox, D. J.; Keith, T.; Al-Laham, M. A.; Peng, C. Y.; Nanayakkara, A.; Gonzalez, C.; Challacombe, M.; Gill, P. M. W.; Johnson, B.; Chen, W.; Replogle, E. S.; Pople, J. A. Gaussian 98. Gaussian, Inc.: Pittsburgh, 1998.

(22) Stull, D. R.; Prophet, H. *JANAF Thermochemical Tables*, NSRDS−NBS 37, U. S. Government Printing Office: Washington, D. C. **1971**.

(23) Curtiss, L. A.; Redfern, P. C. *J. Chem. Phys.* **1999**, *110*, 4703.

(24) Pitzer, K. S.; Gwinn, W. *J. Chem. Phys*. **1942**, *10*, 428.

(25) Fulle, D.; Hamann, H. F.; Hippler, H.; Jänsch, C. P. *Ber. Bunsen-Ges. Phys. Chem.* **1997**, *101*, 1433.

(26) Gurvich, L. V.; Veyts, I. V.; Alcock, C. B. *Thermodynamic Properties of Individual Substances*, 4th ed.; Hemisphere: New York, 1992, Vol. 2.

(27) Cohen, N. *Int. J. Chem. Kinet*. **1982**, *14*, 1339.

(28) Cohen, N.; Westburgh, K. R. *Int. J. Chem. Kinet*. **1986**, *18*, 99.

(29) Cohen, N. *Int. J. Chem. Kinet*. **1989**, *21*, 909.

(30) Westmoreland, P. R. *Combust. Sci. Technol.* **1992**, *82*, 151.

(31) Bozzelli, J. W.; Dean, A. M.; Ritter, E. R. *Combust. Sci. Technol.* **1991**, *80*, 63.

(32) (a) Gilbert, R. G.; Smith, S. C. *Theory of Unimolecular and Recombination Reactions*; Oxford Press: New York, 1990. (b) Gilbert, R. G.; Smith, S. C.; Jordan, M. J. T. *Unimol Program Suite*, 1993. (c) Gilbert, R. G.; Luther, K.; Troe, J. *Ber. Bunsen-Ges. Phys. Chem.* **1983**, *87*, 169.

(33) Knyazev, V. D.; Tsang, W. *J. Phys. Chem. A* **2000**, *104*, 10 747.

(34) Barat, R. B.; Bozzelli, J. W. *J. Phys. Chem.* **1992**, *96*, 2494.

(35) Knyazev, V. D.; Kalinovski, I. J.; Slagle, I. R. *J. Phys. Chem. A* **1999**, *103*, 3216.

(36) Canosa-Mas, C. E.; Dillon, T. J.; Sidebottom, H.; Thompson, K. C.; Wayne, R. P. *Phys. Chem. Chem. Phys.* **2001**, *3*, 542.

(37) Kleindienst, T. E.; Shepson, P. B.; Nero, C. M.; Bufalini, J. *Int. J. Chem. Kinet*. **1989**, *21*, 863.

(38) Werner, J. H.; Cool, T. A. *Combust. Flame* **1999**, *120*, 125.

(39) Taylor, P. H.; Sidhu, S. S.; Rubey, W. A.; Dellinger, B.; Wehrmeier, A.; Lenoir, D.; Schramm, K.-W. *Proc. Combust. Inst.* **1998**, *27*, 1769.

(40) Wehrmeier, A.; Lenoir, D.; Sidhu, S. S.; Taylor, P. H.; Rubey, W. A.; Kettrup, A.; Dellinger, B. *Environ. Sci. Technol.* **1998**, *32*, 2741.

(41) Taylor, P. H.; Wehrmeier, A.; Sidhu, S. S.; Lenoir, D.; Schramm, K.-W.; Kettrup, A. *Chemosphere* **2000**, *40*, 1297.